Journal of Alloys and Compounds 509 (2011) 7229–7237

Contents lists available at ScienceDirect

Journal of Alloys and Compounds

journal homepage: www.elsevier.com/locate/jallcom

# Effect of ball milling the hybrid reinforcements on the microstructure and mechanical properties of Mg–(Ti + $n$-$Al_2O_3$) composites

S. Sankaranarayanan, S. Jayalakshmi, M. Gupta *

*Department of Mechanical Engineering, National University of Singapore (NUS), 9 Engineering Drive 1, Singapore 117576, Singapore*

ARTICLE INFO

*Article history:*
Received 16 March 2011
Received in revised form 14 April 2011
Accepted 15 April 2011
Available online 23 April 2011

*Keywords:*
Metal matrix composites
Mechanical alloying
Rapid solidification
Microstructure
Mechanical properties
Scanning electron microscopy (SEM)

ABSTRACT

In this study, composites containing pure magnesium and hybrid reinforcements (5.6 wt.% titanium (Ti) particulates and 2.5 wt.% nanoscale alumina ($n$-$Al_2O_3$) particles) were synthesized using the disintegrated melt deposition technique followed by hot extrusion. The hybrid reinforcement addition into the Mg matrix was carried out in two ways: (i) by direct addition of the reinforcements into the Mg–matrix, Mg–(5.6Ti + 2.5$n$-$Al_2O_3$) and (ii) by pre-synthesizing the composite reinforcement by ball milling and its subsequent addition into the Mg–matrix, Mg–(5.6Ti + 2.5$n$-$Al_2O_3$)$_{BM}$. Microstructural characterization revealed significant grain refinement due to reinforcement addition. The evaluation of mechanical properties indicated a significant improvement in microhardness, tensile and compressive properties of the composites when compared to monolithic magnesium. For the Mg–(5.6Ti + 2.5$n$-$Al_2O_3$) composite, wherein the reinforcements were directly added into the matrix, the improvement in strength properties occurred at the expense of ductility. For the Mg–(5.6Ti + 2.5$n$-$Al_2O_3$)$_{BM}$ composites with pre-synthesized ball-milled reinforcements, the increase in strength properties was accompanied by an increase/retention of ductility. The observed difference in behaviour of the composites is primarily attributed to the morphology and distribution of the reinforcements obtained due to the ball-milling process, thereby resulting in composites with enhanced toughness.



## 1. Introduction

In recent years, the increasing requirements for improved fuel economy and emission reduction have resulted in the development of light weight materials [1–4]. Magnesium (Mg) with a density of 1.74 g/cc (~35% lighter than aluminium) is an excellent choice for weight critical applications. It exhibits dimensional stability, good machinability, excellent damping capacity and high specific mechanical properties [4–6]. However, the use of Mg-alloys in critical industrial and commercial applications is restricted due to their limited ductility and toughness, which is attributed to the limited slip systems in the hexagonal closed packed (HCP) crystal structure of Mg [5–7]. Most of these limitations can be overcome by judicious incorporation of high strength and high modulus reinforcements into Mg–matrix either in the form of fibers or particles. The introduction of such reinforcements into the Mg–matrix significantly improves the specific mechanical properties like tensile strength, elastic modulus and yield strength, at the expense of ductility [2,3,8]. The available literature reveals that simultaneous enhancement in strength and ductility of Mg composite can be achieved by the addition of reinforcements such as alumina, SiC or CNT in nanometer scale [9–14]. Recent works have identified that addition of hybrid reinforcements positively influence the mechanical properties of the Mg–composites [15–18]. In these works, the hybrid reinforcements were prepared using mechanical alloying [9,18]. Hence, the end properties of Mg–MMCs would be strongly influenced by factors such as: the type of primary [19] and secondary processing [20], the matrix constituents and their type [2,3], shape and volume fraction of the reinforcements and the method of reinforcement preparation [21–23].

In this work, pure Mg has been incorporated with hybrid reinforcements containing 5.6 wt.% Ti and 2.5 wt.% nanoscale alumina particles (5.6Ti + 2.5$n$-$Al_2O_3$). The primary aim of this work is to study the effect of ball milling the hybrid reinforcements on the properties of Mg–MMCs. Hybrid reinforcement addition was carried out by two means. (i) By addition of Ti and $n$-$Al_2O_3$ particles directly into the matrix and (ii) by pre-synthesizing Ti and $n$-$Al_2O_3$ particles using ball milling and their subsequent addition to the Mg–matrix. The composites were produced by the disintegrated melt deposition technique (DMD) and hot extruded for further characterization [24–26]. Physical, microstructural and mechanical properties of the Mg–(Ti + $n$-$Al_2O_3$) MMCs were evaluated in order to study the effect of reinforcement ball milling on the properties.

* Corresponding author. Tel.: +65 6516 6358; fax: +65 6779 1459.
*E-mail address:* mpegm@nus.edu.sg (M. Gupta).

0925-8388/$ – see front matter © 2011 Elsevier B.V. All rights reserved.
doi:10.1016/j.jallcom.2011.04.083

**Table 1**
Density, porosity and microstructural properties of Mg and Mg-composites.

| Materials | Density | | | Microstructure | |
|---|---|---|---|---|---|
| | Theoretical density (g/cc) | Experimental density (g/cc) | Porosity (%) | Grain size (μm) | Aspect ratio |
| Pure Mg | 1.7400 | 1.7129 ± 0.0015 | 0.02 | 21.30 ± 2.60 | 1.633 ± 0.44 |
| Mg–($5.6Ti_p + 2.5Al_2O_3$) | 1.8481 | 1.6755 ± 0.0255 | 0.09 | 14.88 ± 1.55 | 1.679 ± 0.51 |
| Mg–($5.6Ti_p + 2.5Al_2O_3$)$_{BM}$ | 1.8481 | 1.7826 ± 0.0173 | 0.04 | 7.64 ± 1.47 | 1.710 ± 0.63 |

## 2. Experimental procedures

### 2.1. Materials

Mg turnings of >99.9% purity supplied by ACROS Organics, New Jersey, USA were used as the matrix material. Elemental Ti of particle size <140 μm, purity 98% and *n*-$Al_2O_3$ particulates of particle size ~50 nm supplied by Merck and Baikowski, Japan respectively were used as particulate reinforcements.

### 2.2. Processing

#### 2.2.1. Preparation of reinforcements

Based on our previous works [25,26], the best composition of Ti and *n*-$Al_2O_3$ reinforcement in Mg matrix were identified as 5.6 wt.% and 2.5 wt.% respectively, and was chosen for the present investigation. Initially, prior to ball milling, the elemental Ti and *n*-$Al_2O_3$ particles were blended with 0.3 wt.% stearic acid (process control agent) for 1 h using a Retsch PM-400 mechanical alloying machine to ensure uniform distribution of Ti and n-$Al_2O_3$ particles. After blending, steel balls were added and the blended mixture was ball milled for 2 h. Ball milling was carried out so that the nanosize *n*-$Al_2O_3$ particles effectively get embedded in the micron size Ti particles [18,27,28]. The ball to powder weight ratio was kept at 20:1 and the speed of the milling machine was set at 200 rpm during the blending and ball milling processes [18].

#### 2.2.2. Primary processing

Monolithic and reinforced Mg composites were synthesized through the innovative DMD method [24]. Reinforcements used were (1) elemental Ti and nano-alumina particulates, herein denoted as ($5.6Ti + 2.5n$-$Al_2O_3$) and (2) ball milled mixture of Ti and nano-alumina, herein denoted as ($5.6Ti + 2.5n$-$Al_2O_3$)$_{BM}$ respectively. The Mg turnings together with the reinforcement particulates were heated in a graphite crucible to 750 °C in an electrical resistance furnace, under inert argon gas protective atmosphere. The superheated molten slurry was stirred for 5 min at 460 rpm using a twin blade (pitch 45°) mild steel impeller to facilitate the uniform distribution of reinforcement particulates in the metallic matrix. The impeller was coated with Zirtex 25 (86% $ZrO_2$, 8.8% $Y_2O_3$, 3.6% $SiO_2$, 1.2% $K_2O$ and $Na_2O$, and 0.3% trace inorganic) to avoid iron contamination of the molten metal. The melt was then released through a 10 mm diameter orifice at the base of the crucible. The composite melt was disintegrated by two jets of argon gas oriented normal to the melt stream and located 265 mm from the melt pouring point. The disintegrated composite melt slurry was subsequently deposited onto a metallic substrate located 500 mm from the disintegration point. The argon gas flow rate was maintained at ~25 l/min. An ingot of 40 mm diameter was obtained following the deposition stage. The synthesis of monolithic Mg was carried out using steps similar to those employed for the reinforced materials except that no reinforcement particulates were added.

#### 2.2.3. Secondary processing

The monolithic Mg and the particulate reinforced Mg-composites obtained from the DMD process were machined to a diameter of 36 mm and soaked at 400 °C for 60 min prior to extrusion. Hot extrusion was then carried out using a 150 T hydraulic press at 350 °C with an extrusion ratio of 20.25:1 to obtain rods of 8 mm in diameter.

### 2.3. Density measurements

The experimental mass densities of as-polished extruded monolithic Mg and Mg-composites were determined using Archimedes' principle. This involved weighing the sample in air and then in distilled water using an A&D ER-182A electronic balance with an accuracy of ±0.0001 g. The theoretical densities of composites were calculated using the rule of mixtures [24–26].

### 2.4. Microstructural characterization

The grain morphology and the distribution of reinforcements in Mg matrix were studied on as-polished samples. A Hitachi S-4300 field emission scanning electron microscope (FESEM) equipped with energy dispersive X-ray spectroscopy (EDS), an Olympus metallographic optical microscope and Scion image analysis software were used for this purpose. The microstructure of the as-received Ti particulates and ball milled (Ti + *n*-$Al_2O_3$) particulates were also investigated for determining the average particle size and particle morphology.

### 2.5. X-ray diffraction studies

X-ray diffraction (XRD) analysis was carried out on polished samples of monolithic pure Mg, its composites and the ball milled hybrid reinforcements using an automated Shimadzu LAB-X XRD-6000 diffractometer. The samples were exposed to Cu Kα radiation (λ = 1.54056 Å) at a scanning speed of 2°/min. The Bragg angles and the values of interplanar spacing, *d*, obtained were matched with standard values for Mg, Ti, *n*-$Al_2O_3$ and other related phases.

### 2.6. Coefficient of thermal expansion

An INSEIS TMA PT 1000LT thermo-mechanical analysis instrument was used to determine the coefficients of thermal expansion (CTE) of the as-extruded monolithic Mg and composite samples. Heating rate of 5 °C/min was maintained. Argon gas flow rate was maintained at 100 ccm/min. Displacement of the test samples (each 5 mm long) as a function of temperature (50–400 °C) was measured using an alumina probe and was subsequently used to determine the CTE.

### 2.7. Microhardness measurements

The microhardness measurements were carried out on the as-polished samples of extruded monolithic Mg and its composites using Matsuzawa MXT 50 automatic digital micro-hardness tester. Vickers indenter under a test load of 25 gf and a dwell time of 15 s was used to perform the micro hardness tests in accordance with the ASTM standard E3 84-99. The tests were conducted on three samples for each composition for 10–15 repeatable readings.

### 2.8. Tensile behaviour

A fully automated servo-hydraulic mechanical testing machine, Model-MTS 810 was used to determine the tensile properties of the as-extruded Mg and composites samples in accordance with ASTM test method E8M-96. The crosshead speed was set at 0.254 mm/min. The dimensions of tension test specimens were 5 mm diameter and 25 mm gauge length. Instron 2630–100 series clip-on type extensometer was used to measure the failure strain. The work of fracture was determined using the excel software from the stress versus strain curves obtained from the testing results. For each composition, a minimum of 5 tests were conducted to obtain repeatable values.

### 2.9. Compressive behaviour

The compressive properties of the as-extruded Mg and composites samples were determined in accordance with ASTM test method E9-89a using MTS 810 testing machine with a crosshead speed set at 0.04 mm/min on round compressive test specimens of 8 mm diameter. Ratio of length to diameter for all the samples was ~1. The work of fracture was determined using the excel software from the stress versus strain curves obtained from the testing results. For each composition, a minimum of 5 tests were conducted to obtain repeatable values.

### 2.10. Fracture behaviour

The fracture surface analyses of the monolithic alloy and composites tested under tension and compression were accomplished using a Hitachi S-4300 FESEM.

## 3. Results

### 3.1. Macrostructure

The macrostructural observation of the as-cast ingot and extruded rods did not reveal any macrostructural defects such as cracks, pores, blow holes, etc. The surface of both as-cast ingot and extruded rods were smooth and free from any circumferential defects.

**Table 2**
CTE and Microhardness values of Mg and Mg-composites.

| Material | CTE (μm/mK) | Micro hardness |
|---|---|---|
| Pure Mg | 28.52 | 48 ± 1 |
| Mg–($5.6Ti_p + 2.5Al_2O_3$) | 23.73 | 74 ± 2 |
| Mg–($5.6Ti_p + 2.5Al_2O_3$)$_{BM}$ | 23.53 | 69 ± 1 |

### 3.2. Density measurements

The results of density measurements conducted on the extruded unreinforced monolithic magnesium and reinforced Mg-composites are shown in Table 1. The volumetric porosity was calculated from the theoretical and experimental density values. The porosity level of Mg–(5.6Ti + 2.5*n*-$Al_2O_3$)$_{BM}$ composite were found to be less when compared to Mg–(5.6Ti + 2.5*n*-$Al_2O_3$) composite. The porosity level in both the reinforced composites was found to be marginally higher than that of monolithic Mg. However, the porosity levels observed in all the samples are relatively very low (<0.1%).

### 3.3. Microstructural characterization

The grain characteristics of monolithic Mg and the composites as seen in Fig. 1(a–c) are listed in Table 1. The average grain size of both the composites is smaller than that of the monolithic Mg and the Mg–(5.6Ti + 2.5*n*-$Al_2O_3$)$_{BM}$ composite exhibited the lowest grain size. The microstructures as seen in Fig. 2(a and b) reveal relatively uniform distribution of reinforcements in the Mg–(5.6Ti + 2.5*n*-$Al_2O_3$)$_{BM}$ composite when compared to Mg–(5.6Ti + 2.5*n*-$Al_2O_3$) composite. The Ti particulates are found clustered in the Mg–(5.6Ti + 2.5*n*-$Al_2O_3$) composite and the *n*-$Al_2O_3$ particles are found distributed in the matrix Fig. 2(c). In the Mg–(5.6Ti + 2.5*n*-$Al_2O_3$)$_{BM}$ composite shown in Fig. 2(d), the *n*-$Al_2O_3$ particles were found adhered to the Ti particulates. The uneven particle size of the as-received Ti particulate is evident from the microstructure and image analysis results, whereas in the ball milled (5.6Ti + 2.5*n*-$Al_2O_3$) powder, relatively uniform-sized particle are seen, as shown in Fig. 2(e–h). The microstructure results also revealed that the as-received Ti consists of more number of sharp edged particles whereas the ball milled (Ti + *n*-$Al_2O_3$) powder contains Ti particles with blunted corners and rounded edges.

### 3.4. X-ray diffraction studies

The results of XRD studies conducted on the composite samples and the ball milled powder is shown in Fig. 3. In the ball-milled powder, Ti and *n*-$Al_2O_3$ peaks are observed. In both the composites, although the Ti and *n*-$Al_2O_3$ peaks were observed, the peaks were not prominent. This is due to their relatively low volume fraction in the Mg matrix. However, the presence of these reinforcements was confirmed from the microstructural investigation, as seen earlier in Fig. 2(c–g). In both the ball-milled powder and the composites, no interfacial reaction products arising due to the interaction between Ti–$Al_2O_3$ and Mg–$Al_2O_3$ are observed. This could possibly be due to the very low volume fraction of the phases (<2% $V_f$, if formed), which would remain undetected by the technique of XRD.

### 3.5. Coefficient of thermal expansion

The thermal expansion coefficients of monolithic Mg and composites were experimentally determined as shown in Table 2. The results show a marginal improvement in dimensional stability (i.e. reduction in CTE values) in both the composites due to the presence of the reinforcements.

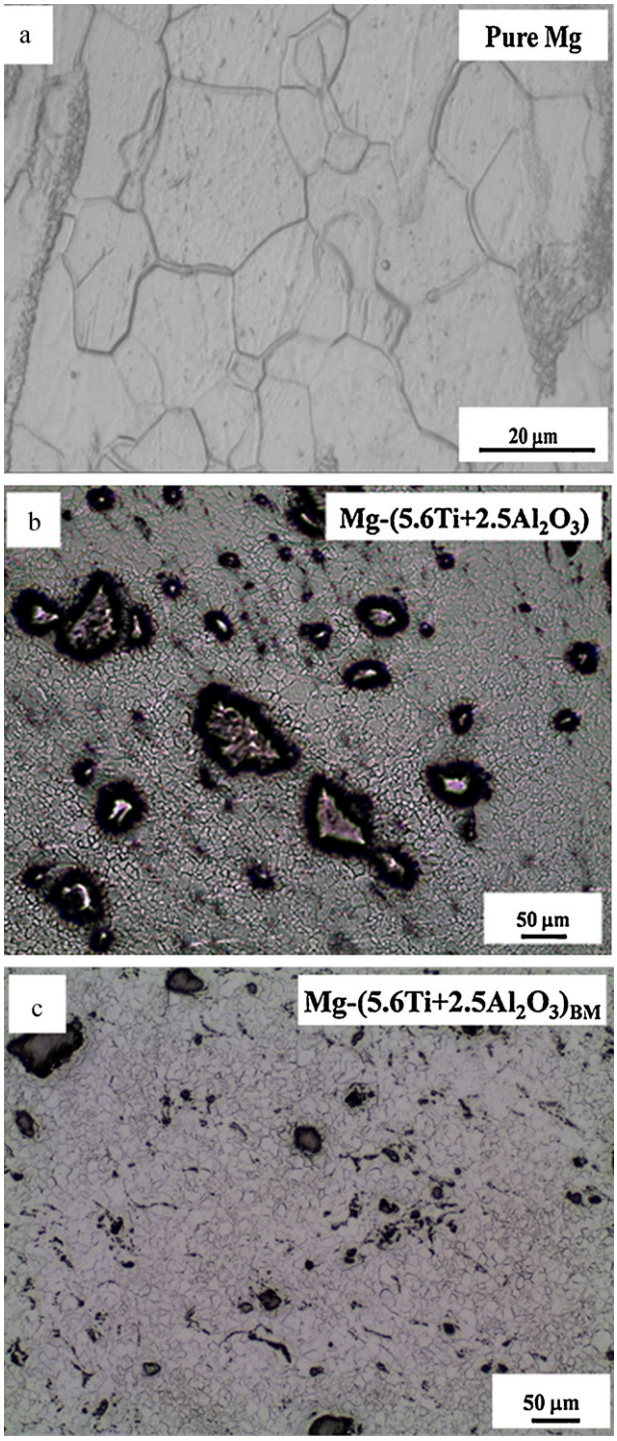


**Fig. 1.** Representative optical micrographs showing the grain morphology of (a) monolithic Mg, (b) Mg–(5.6Ti + 2.5$Al_2O_3$) composite and (c) Mg–(5.6Ti + 2.5$Al_2O_3$)$_{BM}$ composite.

### 3.6. Hardness measurements

The results of the microhardness measurements (Table 2) show a significant increase in hardness value in both the composites, when compared to the monolithic Mg. Among the composites, the Mg–(5.6Ti + 2.5*n*-$Al_2O_3$) composite shows relatively

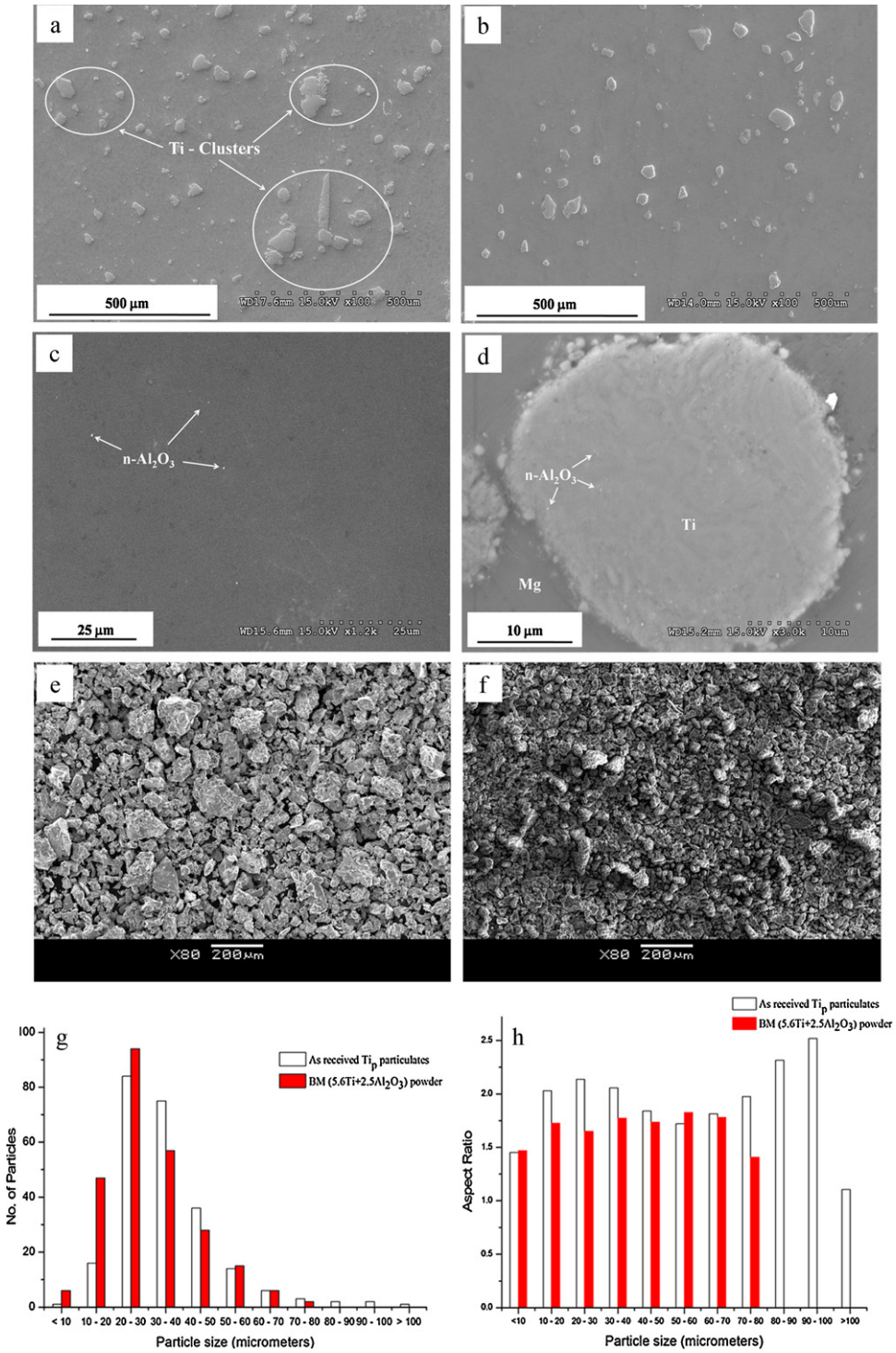


**Fig. 2.** Representative SEM micrographs showing (a) distribution of uneven sized Ti particulate clusters in Mg–(5.6Ti + 2.5$Al_2O_3$) composite, (b) distribution of Ti particulates in Mg–(5.6Ti + 2.5$Al_2O_3$)$_{BM}$ composite, (c) presence of *n*-$Al_2O_3$ in Mg–(5.6Ti + 2.5$Al_2O_3$) composite, (d) *n*-$Al_2O_3$ embedded in Ti particulates in Mg–(5.6Ti + 2.5$Al_2O_3$)$_{BM}$ composite, (e) as received Ti particulates and (f) ball milled (5.6Ti + 2.5$Al_2O_3$) powder. Graphs showing the distribution of (g) no. of particles vs. particle size and (h) particles aspect ratio vs. particle size.

higher mean hardness values than the Mg–(5.6Ti + 2.5*n*-$Al_2O_3$)$_{BM}$ composite.

### 3.7. Tensile behaviour

The results of tensile test as seen in Fig. 4 and Table 3 reveal a significant improvement in yield strength (0.2% YS) of >30% and >25% improvement in ultimate tensile strength (UTS) in both the composite samples when compared to the monolithic Mg. However, the increase in strength in Mg–(5.6Ti + 2.5*n*-$Al_2O_3$) composite is accompanied by ~50% reduction in ductility. Interestingly, the failure strain of the Mg–(5.6Ti + 2.5*n*-$Al_2O_3$)$_{BM}$ composite did not show any loss of ductility, and the mean fracture strain values are even slightly higher than that of monolithic Mg. The composites with ball-milled hybrid reinforcements hence exhibit better overall performance under tensile loading.

**Table 3**
Tensile properties of pure magnesium and those reinforced with hybrid reinforcements.

| Material | 0.2% YS (MPa) | UTS (MPa) | Failure strain (%) | WoF[a] (J/m$^3$) |
|---|---|---|---|---|
| Pure Mg | 125 ± 9 | 169 ± 11 | 6.2 ± 0.7 | 10.3 ± 1.1 |
| Mg–($5.6Ti_p$ + $2.5Al_2O_3$) | 175 ± 4 | 227 ± 10 | 3.3 ± 0.2 | 7.3 ± 0.5 |
| Mg–($5.6Ti_p$ + $2.5Al_2O_3$)$_{BM}$ | 168 ± 8 | 214 ± 8 | 6.8 ± 0.8 | 14.4 ± 2.6 |

[a] Values calculated from the stress–strain diagram using excel software.

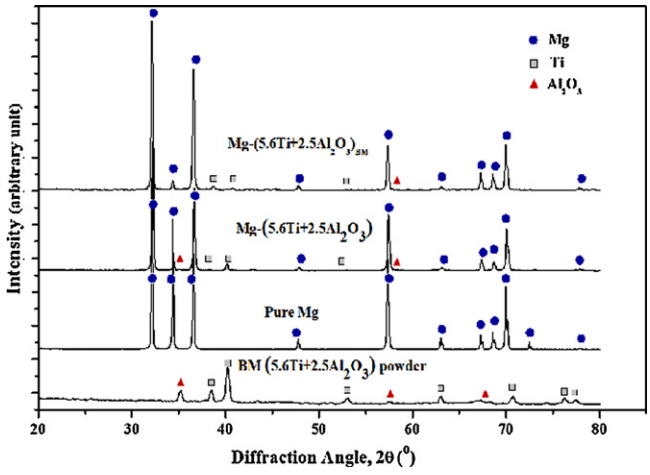


**Fig. 3.** XRD diffraction pattern of ball milled powder, monolithic Mg and its hybrid composites.

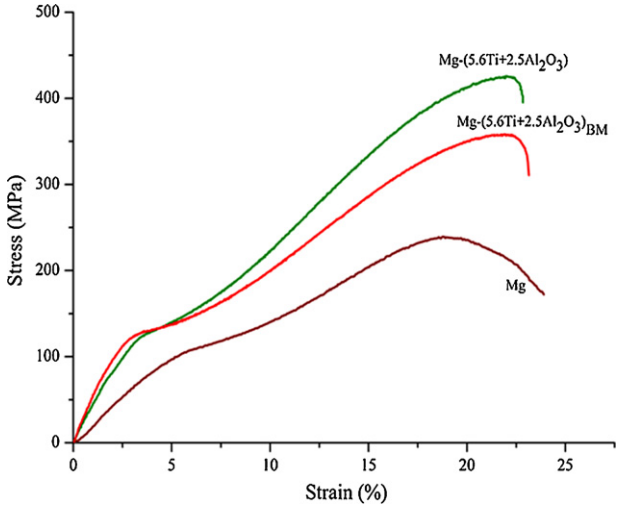


**Fig. 5.** Compressive stress–strain curves of monolithic Mg and its hybrid composites.

### 3.8. Compressive behaviour

The compression test results as shown in Fig. 5 and Table 4 indicate an increase of >20% in the compressive yield strength (0.2% CYS) and >45% in ultimate compressive strength (UCS) for both the composites. The work of fracture of the composites also improves significantly when compared to monolithic Mg. The hybrid composite incorporated with the direct additions of reinforcements show better overall compressive strength properties than the hybrid composite reinforced with ball milled reinforcements.

### 3.9. Fracture behaviour

The tensile fracture surfaces of Mg and Mg composites are shown in Fig. 6(a–e). The fracture surface of monolithic Mg samples

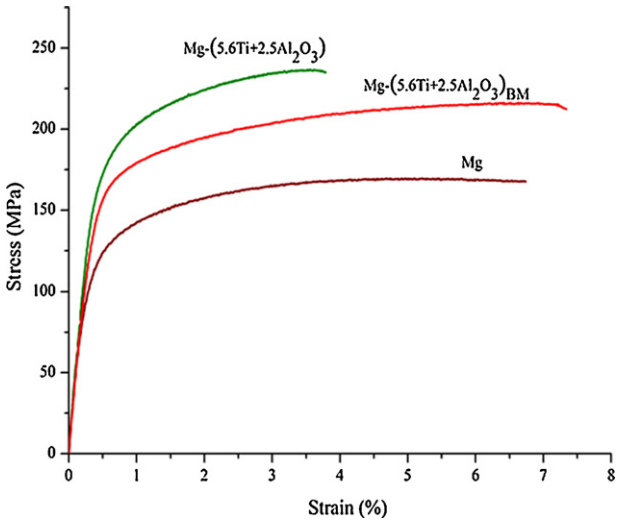


**Fig. 4.** Tensile stress–strain curves of monolithic Mg and its hybrid composites.

indicates a cleavage mode of fracture (Fig. 6a). Tensile fractographs of Mg–(5.6Ti + 2.5*n*-$Al_2O_3$) reveal brittle features (Fig. 6(b and c)), while the fracture surfaces of Mg–(5.6Ti + 2.5*n*-$Al_2O_3$)$_{BM}$ hybrid composites show prominent ductile features due to plastic deformation ((Fig. 6(d and e)). Under compressive loading conditions, fracture surface analysis of monolithic Mg and its composites samples reveal the presence of shear bands as shown in Fig. 7(a–c).

## 4. Discussion

### 4.1. Synthesis

The monolithic and reinforced Mg composites were successfully synthesized by the DMD process followed by hot extrusion. Absence of any macrodefects clearly indicate the suitability of processing parameters used in this study [24,29]. The oxidation of Mg melt was prevented by the inert Ar gas atmosphere and there was no reaction detected between the Mg melt/composite slurries with the graphite crucible [24,25]. This can be attributed to the inability of Mg to form stable carbides. The characterization results clearly indicate the feasibility of the DMD process as a potential fabrication technique for hybrid Mg composites containing Ti and *n*-$Al_2O_3$ particulates [24].

### 4.2. Microstructure

The microstructures of pure Mg and its composites (Figs. 1 and 2) were studied in terms of: (i) porosity, (ii) morphology of reinforcements and its distribution in the Mg matrix, (iii) grain size and morphology, and (iv) matrix–reinforcement interfacial characteristics.

Among the composites, the slight increase in the volume percentage of porosity in Mg–(5.6Ti + 2.5*n*-$Al_2O_3$) composite can be attributed to the formation of metal free zones at the sharp corners

**Table 4**
Compressive properties of pure magnesium and those reinforced with hybrid reinforcements.

| Material | 0.2% CYS (MPa) | UCS (MPa) | Failure strain (%) | WoF[a] (J/m$^3$) |
|---|---|---|---|---|
| Pure Mg | 87 ± 4 | 240 ± 9 | 19.2 ± 0.7 | 39.0 ± 2.3 |
| Mg–($5.6Ti_p$ + $2.5Al_2O_3$) | 106 ± 0 | 424 ± 15 | 14.4 ± 1.2 | 54.4 ± 5.1 |
| Mg–($5.6Ti_p$ + $2.5Al_2O_3$)$_{BM}$ | 106 ± 3 | 349 ± 9 | 15.2 ± 1.7 | 45.7 ± 5.0 |

[a] Values calculated from the stress–strain diagram using excel software.

of Ti particulates as a result of the inability of high viscosity particulate-molten alloy slurry to negotiate the sharp corners [30].

Considering the reinforcement morphology, the presence of Ti particulate clusters found in the Mg–(5.6Ti + 2.5*n*-$Al_2O_3$) composite (Fig. 2(a)) and a relatively uniform distribution of Ti particulates in the Mg–(5.6Ti + 2.5*n*-$Al_2O_3$)$_{BM}$ composite (Fig. 2(b)) can be attributed to the difference in processing of reinforcement particulates. The as-received Ti particles used directly in Mg–(5.6Ti + 2.5*n*-$Al_2O_3$) composite were characterized by the presence of sharp edges. Further, due to the direct addition, the *n*-$Al_2O_3$ particles in the Mg–(5.6Ti + 2.5*n*-$Al_2O_3$) composite get distributed in the Mg–matrix as seen in Fig. 2(c). In comparison, the ball milled powder had blunted corners as seen in Fig. 2(e and f). This is due to the step of ball milling which led to the blunting of the sharp corners of Ti particles. It may be noted that the ball milling process involves repeated flattening, coldwelding and fracture of particulates [27]. In the process, the *n*-$Al_2O_3$ particles also get embedded into the Ti particulates as seen in Fig. 2(d) [18,27]. From Fig. 2(g), it is observed that the particle sizes in the as-received powder used in the Mg–(5.6Ti + 2.5*n*-$Al_2O_3$) composite varied between 10 and 100 μm, with more number of particles in the range of 20–50 μm. On the other hand, the ball-milled powders had very few Ti particles in the range >70 μm. Also, the number of particles in the range <30 μm increased. The breaking down of bigger size Ti particles to smaller particles during ball milling contributed to the increase in number of smaller size Ti particulates, that eventually reduced the aspect ratio of ball milled (5.6Ti + 2.55*n*-$Al_2O_3$) powder as seen in Fig. 2(h).

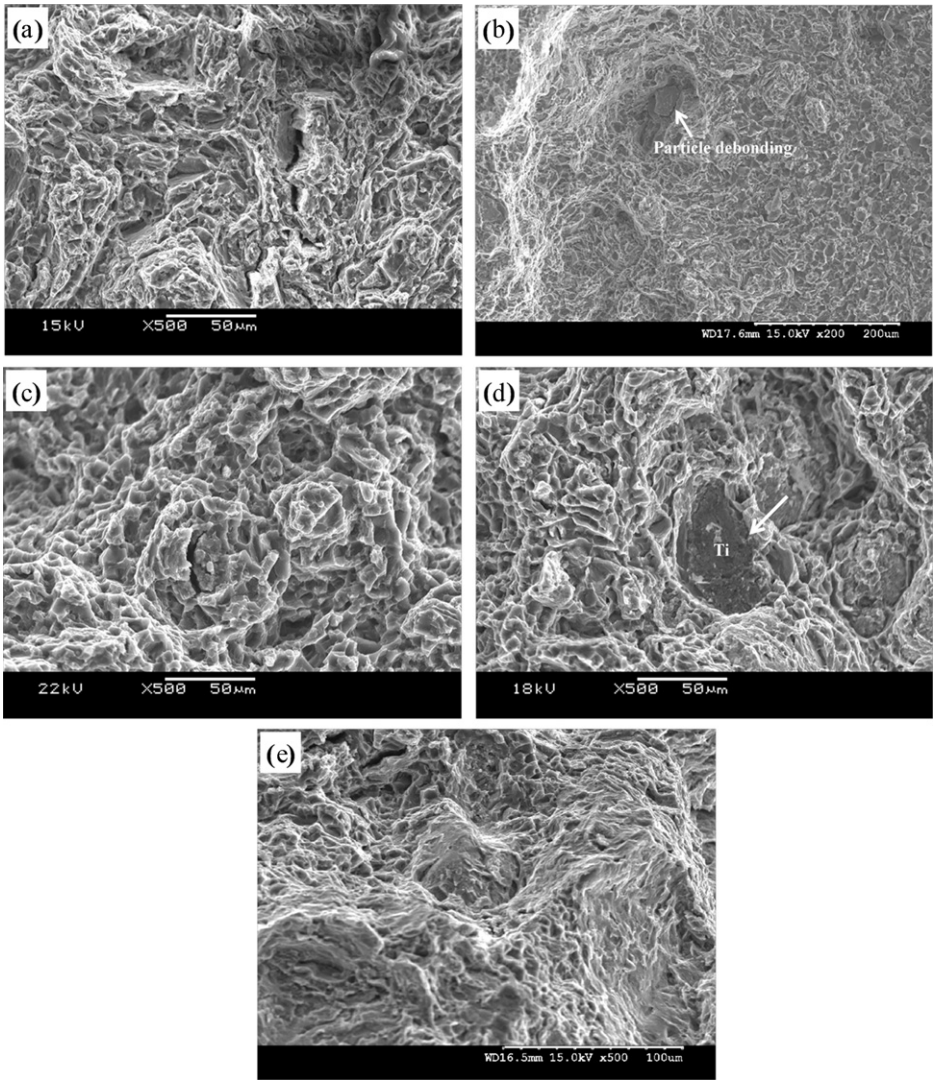


**Fig. 6.** Representative tensile fracture surfaces showing (a) cleavage in monolithic Mg, (b) and (c) particle debonding and brittle features in Mg–(5.6Ti + 2.5$Al_2O_3$) composite, (d) and (e) mixed mode fracture with good particle–matrix interface (arrow) and plastic deformation in Mg–(5.6Ti + 2.5$Al_2O_3$)$_{BM}$ composite.

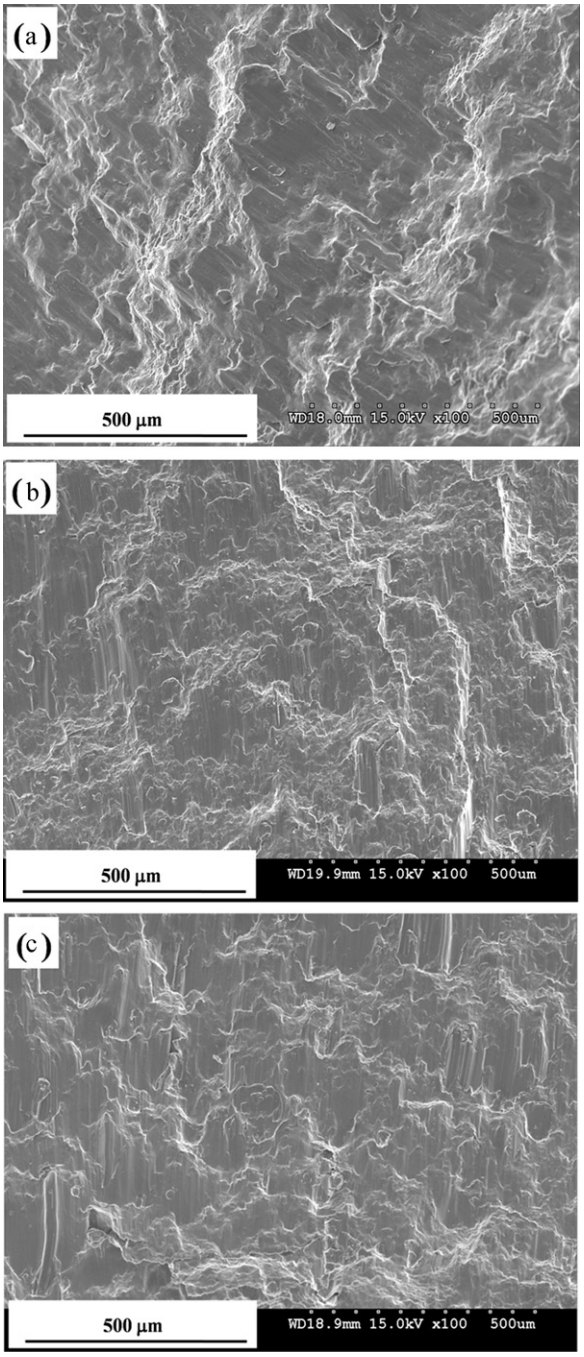


**Fig. 7.** Representative compressive fracture surfaces showing shear bands in (a) monolithic Mg, (b) Mg–(5.6Ti + 2.5$Al_2O_3$) composite and (c) Mg–(5.6Ti + 2.5$Al_2O_3$)$_{BM}$ composite.

The significant grain refinement obtained in the composites as shown in Fig. 1(b and c) can be attributed to the presence of reinforcements and their ability to nucleate Mg-grains during recrystallisation [24,31]. However, among the composites, the Mg–(5.6Ti + 2.5*n*-$Al_2O_3$)$_{BM}$ composite showed the lowest grain size. From Fig. 2, it is observed that the Mg–(5.6Ti + 2.5*n*-$Al_2O_3$)$_{BM}$ composite shows smaller sized reinforcement particles. As smaller particles provide more active sites for Mg-grain nucleation [14], the grain size of the Mg–(5.6Ti + 2.5*n*-$Al_2O_3$)$_{BM}$ is lower than that of Mg–(5.6Ti + 2.5*n*-$Al_2O_3$) composite.

From the XRD phase analyses, it can be inferred that no detectable interfacial product was formed between Mg–$Al_2O_3$ and Ti–$Al_2O_3$. Based on the Mg–Ti phase diagram, there is no intermetallic formation between Mg and Ti [25] and hence the interface between Mg–Ti is free of interfacial products, as seen in Fig. 2(d).

### 4.3. Coefficient of thermal expansion

The marginal improvement in dimensional stability (decrease in CTE) of the composite samples when compared to the monolithic Mg (Table 2) was due to difference in thermal expansion coefficients (CTE) of matrix and reinforcements. The CTE values of Mg, Ti and *n*-$Al_2O_3$ are $27.1 \times 10^{-6}$/K, $9.1 \times 10^{-6}$/K and $7.4 \times 10^{-6}$/K respectively. The low thermal expansion coefficients of reinforcements have reduced the thermal expansion coefficient of the composites [11,23–26]. The experimental CTE values of both the composite samples were determined to be in the same range which indicates that the thermal expansion coefficient is independent of the shape, size and distribution of the reinforcements [32].

### 4.4. Mechanical behaviour

#### 4.4.1. Effect of micro and nanoscale reinforcements

It is well known that the strength properties of metal matrix composite are improved by (i) the inherent properties of the reinforcements such as its high hardness and strength, (ii) grain refinement due to the presence of reinforcements, (iii) obstruction to dislocation movements offered by the reinforcements, and (iv) effective load transfer from the matrix to the reinforcements [3]. Based on earlier works, the micron-size reinforcements improved the strength properties at the expense of ductility [14,21,24], whereas studies on Mg reinforced with nano scale alumina particles indicated that the nano scale particles improved the ductility [14]. This was attributed to the combined effects of grain refinement, uniform distribution of nanosized particulates without agglomeration and slip on extra non-basal slip system [14].

From Table 2, the increase in hardness values in both the composites can be attributed to the presence of relatively harder reinforcements [24–26]. The composites showed ~44% increase in hardness when compared to the unreinforced monolithic Mg. Among the composites, the Mg–(5.6Ti + 2.5*n*-$Al_2O_3$) showed higher mean hardness values when compared to the Mg–(5.6Ti + 2.5*n*-$Al_2O_3$)$_{BM}$ composite, which may be due to the larger number of harder particles and higher aspect ratio of Ti particles (see Fig. 2).

Further, in the present study, mechanical properties characterization indicate that the Mg–(5.6Ti + 2.5*n*-$Al_2O_3$) composite exhibited improved strength properties, but with a drastic reduction in tensile ductility (Table 3). In the Mg–(5.6Ti + 2.5*n*-$Al_2O_3$)$_{BM}$ composite, though the strength was slightly lower, there was no loss of ductility and the composite exhibited increased work of fracture. In both these composites, the volume fraction of reinforcements was kept constant and only the method of hybrid reinforcement preparation was varied. The observed differences in the mechanical behaviour of the two composites indicate that the method of reinforcement preparation also played an important role in defining their behaviour.

These observations clearly indicate that in addition to the above-mentioned strengthening mechanisms, the strength properties of MMCs would also be influenced by factors such as: (a) thermal residual stress between the matrix and the reinforcement [33], which in turn depend on (b) reinforcement morphology [21–23], and (c) reinforcement distribution [34–36] Therefore, a change in the processing method, such as the one employed in Mg–(5.6Ti + 2.5*n*-$Al_2O_3$)$_{BM}$ would bring forth changes in the properties of the reinforcements, which would significantly alter the behaviour of the composite.

*4.4.1.1. Effect of thermal residual stresses.* In metal matrix composites, the differences in thermal expansion coefficients of the

matrix and the reinforcements would result in the introduction of thermal residual stress in the composite [33]. The presence of thermal residual stresses would increase the dislocation density at the particle/matrix interface and hence would contribute to the improvement in the yield strength of the composites. In the present study, the mechanical properties (Tables 3 and 4) show that when compared to monolithic magnesium, the yield strength of the composites has improved significantly, which, as explained above, can be attributed to the increased dislocation density due to reinforcement addition.

Further, Qin and co-workers [21] reported the effect of shape of the reinforcement particles on the residual stresses. It was reported that for near-spherical particles, the residual stress distribution was uniform, while for angular and pointed particles, the stress concentration was higher at the pointed corners [21]. This significantly affected the ductility of the composites. The effect of particle morphology and distribution are discussed in the following sections.

*4.4.1.2. Effect of particle morphology.* The influence of particle shape and size on the mechanical properties of particle reinforced composites has been reported [14,21–23]. It was shown that for sharp edged particles, the stress concentration would occur at the pointed corner of the particle and would increase with the increase in the amount of such sharp edged particles. The presence of such particles in the composite reduced the ductility of the composite [21], and eliminating such particle corners improved the ductility without decreasing the strengthening effect [21]. Further, composites reinforced with smaller size particulate reinforcements exhibited better strength properties than those composites with particles of larger size [14]. Based on the work by Li and Ramesh [23], the aspect ratio of the reinforcement particulates also affected the strength properties of the composites. It was observed that the composites reinforced with higher aspect ratio particulates exhibited improved strength when compared with the composites reinforced with lower aspect ratio particles [23].

From the experimental results obtained in the current investigation (Tables 3 and 4), it can be inferred that due to the presence of many sharp edged particulates in the as-received Ti powder (Fig. 2(e)), the stress concentration is expected to be more at the particle corners in the Mg–(5.6Ti + 2.5$Al_2O_3$) composite than the Mg–(5.6Ti + 2.5$Al_2O_3$)$_{BM}$ composite. In addition, the aspect ratio of the as-received Ti particulates (∼2.1) was found to be relatively higher than the aspect ratio of (5.6Ti + 2.5$Al_2O_3$)$_{BM}$ powder (∼1.6). This is due to the presence of uneven size particulates in the as-received condition Fig. 2(e–h). Thus, the increased stress concentration due to sharp edged particles and the presence of higher aspect ratio particulates resulted in the improvement in strength of Mg–(5.6Ti + 2.5$Al_2O_3$) composite, while also reducing its ductility. On the other hand, in the Mg–(5.6Ti + 2.5$Al_2O_3$)$_{BM}$ composite, ball-milling process ensured relatively larger number of small-sized particles, with smooth/blunt corners and low aspect ratio. The presence of such particles in the Mg–matrix, contributed to the enhanced ductility of the Mg–(5.6Ti + 2.5$Al_2O_3$)$_{BM}$ composite, without decreasing the strengthening effect.

*4.4.1.3. Effect of particle distribution.* The dependence of mechanical behaviour on the particle distribution has been studied earlier and the available literature clearly shows that the homogeneous distribution of reinforcements in the matrix improves the strength and ductility of the composites [34–36]. As the presence of large and sharp particulates would result in particle clustering [34,35], it was reported that such clustering of the reinforcement particles in turn affects the ductility of the composites by enhancing the formation of cracks and their propagation [36].

In the current work, it was observed that the Mg–(5.6Ti + 2.5$Al_2O_3$) composite showed sharp Ti-particulates that were clustered together. Though the $n$-$Al_2O_3$ particles were distributed uniformly in the matrix, under tensile loading, the presence of sharp and clustered Ti particulates in the Mg–(5.6Ti + 2.5$Al_2O_3$) composite have resulted in a drastic reduction in ductility (reduced by ∼50%). In comparison, the Mg–(5.6Ti + 2.5$n$-$Al_2O_3$)$_{BM}$ composite which has blunted, relatively uniformly distributed Ti particulates embedded with $n$-$Al_2O_3$ showed marginally higher ductility and enhanced work of fracture.

Under compressive loading, the Mg–(5.6Ti + 2.5$Al_2O_3$) composite showed higher UCS value than the Mg–(5.6Ti + 2.5$n$-$Al_2O_3$)$_{BM}$ composite. It should be noted that unlike ball-milled reinforcements wherein the $n$-$Al_2O_3$ are found embedded on the Ti particles, in the case of direct addition of reinforcements, both the hard reinforcements ($Ti_p$ and $n$-$Al_2O_3$) are found spatially distributed throughout the matrix. This would give rise to higher load bearing capacity and hence an overall increase in the UCS in the Mg–(5.6Ti + 2.5$Al_2O_3$) composite.

### 4.5. Fracture behaviour

The fracture surface characterization conducted on the tensile fracture samples of monolithic Mg indicated cleavage fracture, which is due to the limited slip systems in the hexagonal closed packed (HCP) crystal structure of Mg [37]. The tensile fracture analysis of Mg–(5.6Ti + 2.5$n$-$Al_2O_3$) and Mg–(5.6Ti + 2.5$n$-$Al_2O_3$)$_{BM}$ composites revealed evidences of brittle fracture Fig. 6(b and c) and mixed mode fracture Fig. 6(d and e), respectively which supported the observed ductility values. The brittleness of the Mg–(5.6Ti + 2.5$n$-$Al_2O_3$) composite can be attributed to the agglomeration, clustering and interface debonding of Ti particulates (arrow in Fig. 6(b)) in the magnesium matrix [17,24]. In Mg–(5.6Ti + 2.5$n$-$Al_2O_3$)$_{BM}$ composite, mixed mode fracture with dominant plastic deformation (Fig. 6(e)) were observed, which corresponds to the uniform distribution of the reinforcements and minimal debonding (arrow in Fig. 6(d)) [17,24,25].

The compression fracture surfaces revealed formation of shear bands in Mg as well as its composites. In all the test samples, fracture occurred at ∼45° angle with respect to the compression test axis. The presence of shear bands indicated twinning, which is the most frequently observed deformation mechanism in Mg-alloys and composites Fig. 7(a–c).

To summarize, based on the present work, it was understood that in addition to the properties of the individual reinforcements and the strengthening mechanisms arising there upon, the method of hybrid reinforcement preparation also played a major role in determining the mechanical response of the developed Mg-composites.

## 5. Conclusions

The following are the conclusions that can be drawn from the present investigation:

(1) DMD technique can successfully synthesize magnesium composites containing hybrid reinforcements (5.6Ti + 2.5$n$-$Al_2O_3$).
(2) The addition of hybrid reinforcements significantly reduced the grain size and CTE and increased the hardness when compared to monolithic Mg.
(3) Hybrid composites prepared by direct addition of the reinforcements, Mg–(5.6Ti + 2.5$n$-$Al_2O_3$), exhibit enhanced strength and reduced ductility under both tensile and compressive loading. This can be attributed to the clustered and angular shaped Ti-particles present in the matrix.

(4) Hybrid composites prepared after ball-milling of the reinforcements, Mg–$(5.6Ti + 2.5n\text{-}Al_2O_3)_{BM}$, exhibit improved strength and relatively minimal variation in ductility under both tensile and compressive loading and when compared to pure magnesium. This can be attributed to the relatively uniform distribution of blunted $(5.6Ti + 2.5n\text{-}Al_2O_3)$ composite particulates.

(5) Among the composites, a relatively higher combination of tensile and compressive strengths were realized when the reinforcement particulates were directly added and a relatively superior ductility was realized when the reinforcement particulates $(5.6Ti + 2.5n\text{-}Al_2O_3)$ were ball milled.

## Acknowledgements

One of the authors, Mr. S. Sankaranarayanan, sincerely thanks the NUS research scholarship for supporting this research for his graduate program.

## References

[1] Karl U. Kainer, Metal Matrix Composites: Custom made Materials for Automotive and Aerospace Engineering, Wiley, 2006.
[2] D.J. Lloyd, Int. Mater. Rev. 39 (1994) 1–23.
[3] I.A. Ibrahim, F.A. Mohamed, E.J. Lavernia, J. Mater. Sci. 26 (1991) 1137–1156.
[4] Hai Zhi Ye, Xing Yang Liu, J. Mater. Sci. 39 (2004) 6153–6171.
[5] M.M. Avedesian, H. Baker, ASM Specialty Handbook. Magnesium and Magnesium Alloys, ASM International, Ohio, 1999.
[6] I.J. Polmear, Mater. Sci. Technol. 10 (1994) 1–16.
[7] G.E. Dieter, Mechanical Metallurgy, McGraw-Hill, USA, 1986.
[8] Luo, Metall. Mater. Trans. A 26A (1995) 2445–2454.
[9] H. Ferkel, B.L. Mordike, Mater. Sci. Eng. A 298 (2001) 193–199.
[10] Hajo Dieringa, J. Mater. Sci. 46 (2011) 289–306.
[11] C.S. Goh, J. Wei, L.C. Lee, M. Gupta, Mater. Sci. Eng. A 423 (2006) 153–156.
[12] S.F. Hassan, M. Gupta:, J. Mater. Sci. 41 (2006) 2229–2236.
[13] S.F. Hassan, M. Gupta, J. Alloys Compd. 457 (2008) 244–250.
[14] S.F. Hassan, M. Gupta, J. Alloys Compd. 419 (2006) 84–90.
[15] Jinhai Gu, Xiaonong Zhang, Mingyuan Gu, J. Alloys Compd. 385 (2004) 104–108.
[16] W.L.E. Wong, M. Gupta, J. Mater. Sci. 40 (2005) 2875–2882.
[17] Sanjay Kumar Thakur, T.S. Srivatsan, Manoj Gupta, Mater. Sci. Eng. A 466 (2007) 32–37.
[18] Meisam K. Habibi, Shailendra P. Joshi, Manoj Gupta, Acta Mater. 58 (2010) 6104–6114.
[19] S.F. Hassan, M. Gupta, Compos. Struct. 72 (2006) 19–26.
[20] K.S. Tun, M. Gupta, J. Mater. Sci. 43 (2008) 4503–4511.
[21] Shuyi Qin, Changrong Chen, Guoding Zhang, Wenlong Wang, Zhongguang Wang, Mater. Sci. Eng. A 272 (1999) 363–370.
[22] V.A. Romanova, R.R. Balokhonov, S. Schmauder, Acta Mater. 57 (2009) 97–107.
[23] Y. Li, K.T. Ramesh, Acta Mater. 46 (16) (1998) 5633–5646.
[24] M Gupta, M.O. Lai, D. Saravanaranganathan, J. Mater. Sci. 35 (2000) 2155–2165.
[25] S.F. Hassan, M. Gupta, J. Alloys Compd. 345 (2002) 246–251.
[26] S.F. Hassan, M. Gupta, Metall. Trans. A 36A (2005) 2253–2258.
[27] C. Suryanarayana, Mechanical Alloying and Milling, CRC Press, New York, 2004.
[28] L. Lu, K.K. Thong, M. Gupta, Compos. Sci. Technol. 63 (2003) 627–632.
[29] L.M. Tham, M. Gupta, L. Cheng, Mater. Sci. Technol. 15 (1999) 1139–1146.
[30] M. Gupta, M.O. Lai, C.Y. Soo, Mater. Res. Bull. 30 (12) (1995) 1525–1534.
[31] M. Gupta, T.S. Srivatsan, J. Mater. Eng. Perform. 8 (4) (1999) 473–478.
[32] R. Arpoĩn, J.M. Molina, R.A. Saravanan, C. Garcıĩa-Cordovilla, E. Louis, J. Narciso, Acta Mater. 51 (2003) 3145–3156.
[33] G. Meijer, F. Ellyin, Z. Xia, Composites B 31 (2000) 29–37.
[34] Zhangwei Wang, Min Song, Chao Sun, Yuehui He, Mater. Sci. Eng. A 528 (2011) 1131–1137.
[35] Slipenyuk, V. Kuprin, Yu. Milmana, J.E. Spowart, D.B. Miracle, Mater. Sci. Eng. A 381 (2004) 165–170.
[36] S. Ahmed, F.R. Jones, Composites 21 (1) (1990) 81–84.
[37] R.E. Reed-hill, Physical Metallurgy Principles, D. Van Nostrand, USA, 1964.